Biochemical and Biophysical Research Communications **290,** 204–212 (2002)
doi:10.1006/bbrc.2001.6173, available online at http://www.idealibrary.com on IDEAL®

Structural Studies of Porcine Myeloid Antibacterial Peptide PMAP-23 and Its Analogues in DPC Micelles by NMR Spectroscopy

Kyoungsoo Park,* Donghoon Oh,* Song Yub Shin,† Kyung-Soo Hahm,‡ and Yangmee Kim*,[1]

**Department of Chemistry, Konkuk University, Seoul 143-701, Korea; †Department of Life Science, Kwangju Institute of Science and Technology, Kwangju 500-712, Korea; and ‡Research Center for Proteineous Materials, Chosun University, Kwangju 501-759, Korea*

Received November 8, 2001

PMAP-23 is a cathelicidin-derived antimicrobial peptide identified from porcine leukocytes. PMAP-23 was reported to show potent antimicrobial activity against Gram-negative and Gram-positive bacteria without hemolytic activity. To study the structure–antibiotic activity relationships of PMAP-23, two analogues by replacing Trp with Ala were synthesized and their tertiary structures bound to DPC micelles have been studied by NMR spectroscopy. PMAP-23 has two α-helices, one from Arg1 to Arg10 in the N-terminal region and the other from Phe18 to Arg23 in the C-terminal region. PMAP-1 ($Trp^{7}\rightarrow Ala$) shows similar structure to PMAP-23, while PMAP-2 ($Trp^{21}\rightarrow Ala$) has a random structure in the C-terminus. PMAP-2 was found to show less antibacterial and vesicle-disrupting activities than PMAP-23 and PMAP-1 [J. H. Kang, S. Y. Shin, S. Y. Jang, K. L. Kim, and K.-S. Hahm (1999) *Biochem. Biophys. Res. Commun.* 264, 281–286]. Trp^{21} in PMAP-23 which induces an α-helical structure in the second α-helix is essential for the antibacterial activity of PMAP-23. Also, the fluorescence data proved that Trp^{21} at the second α-helix is buried deep into the phospholipid in the membrane. Therefore, it implies that Trp^{21} in the second α-helix at the C-terminus of PMAP-23 may play an important role on the interactions with the membrane and the flexible region including two proline residues may allow this α-helix to span the lipid bilayer.

Key Words: **PMAP-23; antibiotic activity; tryptophan; NMR spectroscopy; structure.**

Antimicrobial peptides are a significant component of host defense against invading microbes. They provide immediate protection by direct physicochemical attack on the surface membranes of the microorganisms (1–3). One group of these antimicrobial peptides is the cathelicidins, which have been identified from mammals including human (4–14). Cathelicidin family contain a highly conserved signal sequence and proregion ("cathelin") and a variable antibacterial sequence in the C-terminal domain. Many, but not all, the cathelicidins contain a characteristic elastase cleavage site between the anionic cathelin domain and the cationic C-terminal peptide domain (15). Proteolytic processing at this site has been observed in bovine and porcine neutrophils and was required for microbicidal activity (16, 17). Based on the amino acid composition and structure, the cathelicidin family is classified three groups. The first group contains the amphipathic α-helical peptides such as LL-37, CRAMP, SMAP-29, PMAP-37, BMAP-27, and BMAP-28 (4–9). The second group contains the Arg/Pro-rich or Trp-rich peptides including Bac5, Bac7, PR-39, and indolicidin (10–12). The third group includes Cys-containing peptides such as protegrins (13).

PMAP-23 (RIIDLLWRVRRPQKPKFVTVWVR) was identified from cDNA of porcine myeloid mRNA, and belongs to the amphipathic α-helical peptide group of cathelicidin family (18). PMAP-23 contains highly positively charged 7 residues including 5 arginines and 2 lysines, and 11 hydrophobic residues, and 2 tryptophans. Chemically synthesized PMAP-23 was shown to be microbicidal for representative Gram-negative bacteria and Gram-positive bacteria (18, 19). However, PMAP-23 did not display any hemolytic activity against human erythrocytes even at a concentration of 100 μM, suggesting it has certain degree of target cell membrane selectivity (19).

In the previous study, to investigate the effects of two Trp residues at positions 7 and 21 of PMAP-23 on the antibacterial activity and liposome-disrupting activity, the two analogues (PMAP-1 and PMAP-2) in

[1] To whom correspondence and reprint requests should be addressed. Fax: +82-2-3436-5382. E-mail: ymkim@kkucc.konkuk.ac.kr.

0006-291X/02 $35.00

TABLE 1

Amino Acid Sequences of PMAP-23 and Its Analogues

Peptides	Amino acid sequences	Remarks
PMAP-23	RIIDLLWRVRRPQKPKFVTVWVR-OH	Native peptide
PMAP-1	RIIDLL**A**RVRRPQKPKFVTVWVR-OH	PMAP-23: Trp^{7}→Ala
PMAP-2	RIIDLLWRVRRPQKPKFVTV**A**VR-OH	PMAP-23: Trp^{21}→Ala

which Ala is substituted for Trp-residue at position 7 or 21 in PMAP-23 were synthesized, respectively (19). Trp^{21}→Ala substitution (PMAP-2) in PMAP-23 resulted in more significant reduction on antibacterial activity and liposome-disrupting activity compared to Trp^{7}→Ala substitution (PMAP-1). This result suggested that Trp^{21} residue of PMAP-23 appears to play more important role in antibiotic activity than its Trp^{7} residue. The differences in antibiotic activities of these two peptides are related to their three-dimensional structures on target cell membranes. Therefore, the tertiary structures of PMAP-23 and its two analogues bound to DPC micelles have been determined by 2D-NMR spectroscopy and are compared to each other. Structure–antibiotic activity relationships of these peptides are discussed in the present study.

MATERIALS AND METHODS

Peptide synthesis. All of the peptides listed in Table 1 were synthesized by the solid phase method using Fmoc (9-fluorenylmethoxycarbonyl)-chemistry (20). For each coupling step, the Fmoc-protected amino acid and coupling reagents were added in a 10-fold molar excess with respect to resin substitution. Coupling (60–90 min) were carried out with dicyclohexylcarbodiimide (DCC) and 1-hydroxybenzotriazole (HOBT) in the presence of *N*-methyl-2-pyrrolidone (NMP). Cleavage from resin and deprotection of the synthesized peptide were carried out with a solution of 90% trifluoroacetic acid, 3% water, 1% triisopropylsilane and 2% each of 1,2-ethanedithiol, thioanisole, and phenol. After repeated precipitation with ether, the crude peptide was purified by a reversed-phase preparative HPLC on a Waters 15-μm Deltapak C_{18} column (19 × 300 mm), using an appropriate 0–60% acetonitrile gradient in 0.1% trifluoroacetic acid. Purity of the purified peptide was checked by the analytical reversed-phase HPLC on a C_{18} column (4.6 × 250 mm, Beckman). The molecular masses of the peptides were confirmed with MALDI (matrix-assisted laser desorption/ionization) mass spectrometer (data not shown).

Circular dichroism (CD) analysis. CD experiments were performed using a J720 spectropolarometer (Tokyo, Japan) using a cell of 1-mm pathlength to determine the secondary structure of the peptides in the membrane-mimetic environments. The CD spectra of the peptides in phosphate buffer, 30% TFE/water solution, 15 mM SDS micelles, and 90 mM DPC micelles were recorded at 25°C in the 190- to 250-nm wavelength range at 0.1 nm intervals. The peptide concentrations were 100 μM. For each spectrum, the data of four scans were averaged and smoothed by the J720/98 system program (Version 120C). CD data were expressed as mean residue ellipticity [θ].

Fluorescence spectroscopy. Fluorescence spectra were recorded on a Perkin–Elmer LS50B luminescence spectrometer. Each peptide (5 μM) was added to 1 mL of 5 mM phosphate buffer (pH 7.4) containing 1.0 mM liposomes. Small unilamellar vesicles (SUVs) composed of PC (phosphatidyl choline) and PC (phosphatidyl choline)/PS (phosphatidylserine) (4:1, w/w) was prepared by sonication method. Phospholipid was dissolved in chloroform and evaporated under a stream of nitrogen to form a thin lipid film. The dried lipid was hydrated in 2 ml of 5 mM phosphate buffer (pH 7.4), and then was diluted with 25 ml of the same buffer. The lipid concentration is about 1.0 mM. The peptide/liposome mixture was incubated at room temperature for 10 min prior to recording spectra. The measurements were performed at an excitation wavelength of 280 nm and emission wavelength of 300 to 400 nm. The bandwidth of excitation and emission was 5 and 3 nm, respectively.

NMR experiments. To investigate the conformation of PMAP-23 and its analogues in a membrane-mimicking environment, all sam-

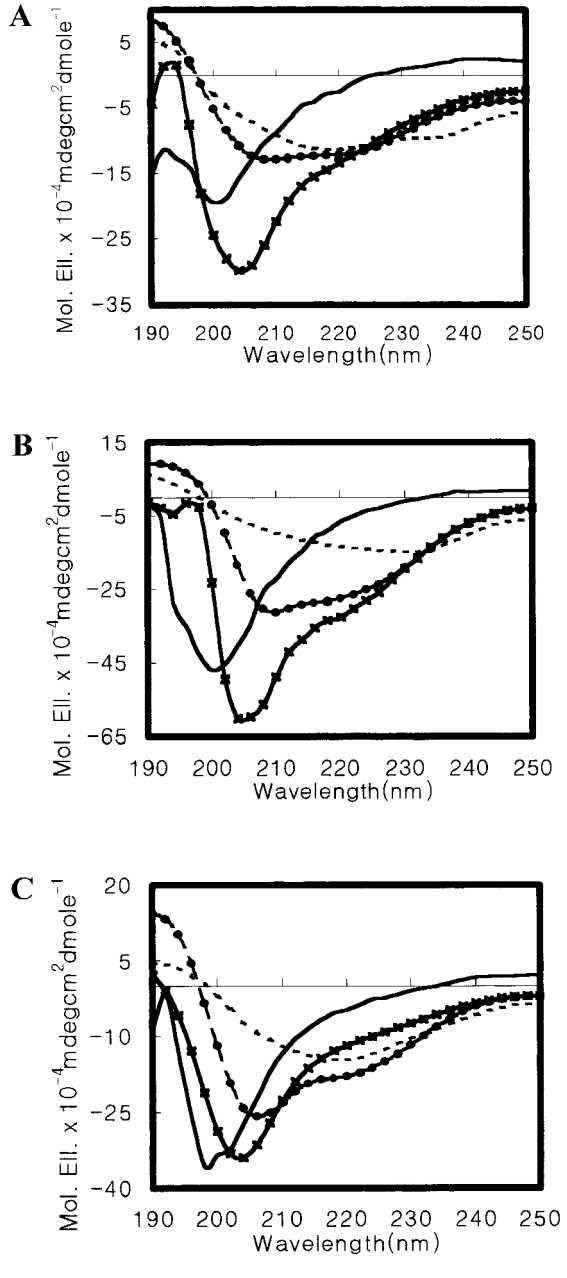

FIG. 1. Circular dichroism spectra of (A) PMAP-23, (B) PMAP-1, and (C) PMAP-2 in H_2O (—), 15 mM SDS micelles (- - -), 30% TFE/H_2O solution (●), and 90 mM DPC micelles (×).

ples for NMR experiments were dissolved in DPC micelles. Perdeuterated dodecyl phosphocholine (DPC-d_{38}) was purchased from Cambridge Isotope Laboratories, Inc. To reduce the possibility of peptide aggregation, we added the DPC in the peptide sample until the best line widths were obtained. About 90 mM DPC micelles were added to the 2 mM peptide sample. All of the phase-sensitive two-dimensional experiments, such as DQF-COSY, TOCSY, PE-COSY, and NOESY were performed using time-proportional phase incrementation method (21–26). For these experiments, 350–512 transients with 2K complex data points were collected for each increment, with a relaxation delay of 1.2–1.5 s between successive transients, and the data along the t_1 dimension were zero-filled to 1K before two-dimensional Fourier transformation. TOCSY experiments were performed using 20, 80, and 100 ms MLEV-17 spin-lock mixing pulses. Mixing times of 150, 250, and, 350 ms were used for NOESY experiments. The PE-COSY experiment was performed using 39° of second pulse to measure the accurate passive coupling constants (26). $^3J_{HN\alpha}$ coupling constants were measured from DQF-COSY spectrum with a spectral width of 4006.41 Hz and digital resolution of 0.98 Hz/point (27). Chemical shifts are expressed relative to DSS signal at 0 ppm. All the spectra were recorded at 293, 303, 313, and 323 on Bruker DPX-spectrometer at Konkuk University. Temperature coefficients were calculated from the TOCSY experiments at three different temperatures (293, 303, and 313K) to investigate the intramolecular hydrogen bondings in the peptides. All NMR spectra were processed off-line using the FELIX software package on SGI (Molecular Simulations Inc., San Diego, CA).

Structure calculation. Distance constraints were extracted from the NOESY spectra with mixing times of 150 and 250 ms. The volumes of the NOEs between the two β protons of Trp residues were used as references. All other volumes were converted into the distances by assuming a simple $1/r^6$ distance dependence. All the NOE intensities are divided into three classes (strong, medium, and weak) with distance ranges of 1.8–2.7, 1.8–3.3, and 1.8–5.0 Å, respectively (28, 29). Structure calculations were carried out using X-PLOR version 3.851 (30) with the topology and parameter sets topallhdg and parallhdg, respectively. Standard pseudoatom corrections were applied to the nonstereospecifically assigned restraints (31) and an additional 0.5 Å was added to the upper bounds for the NOEs involving methyl protons (32). A hybrid distance geometry-dynamical simulated annealing protocol (33, 34) was employed to generate the structures. The target function that is minimized during simulated annealing comprises only quadratic harmonic potential terms for covalent geometry, square-well quadratic potentials for the experimental distance and torsion angle restraints, and a quartic van der Waals repulsion term for the nonbonded contacts. There were no hydrogen-bonding, electrostatic, or 6–12 Lennard–Jones empirical potential energy terms in the target function. Total of 80 structures were generated, 20 structures with the lowest energies were selected for the further analysis.

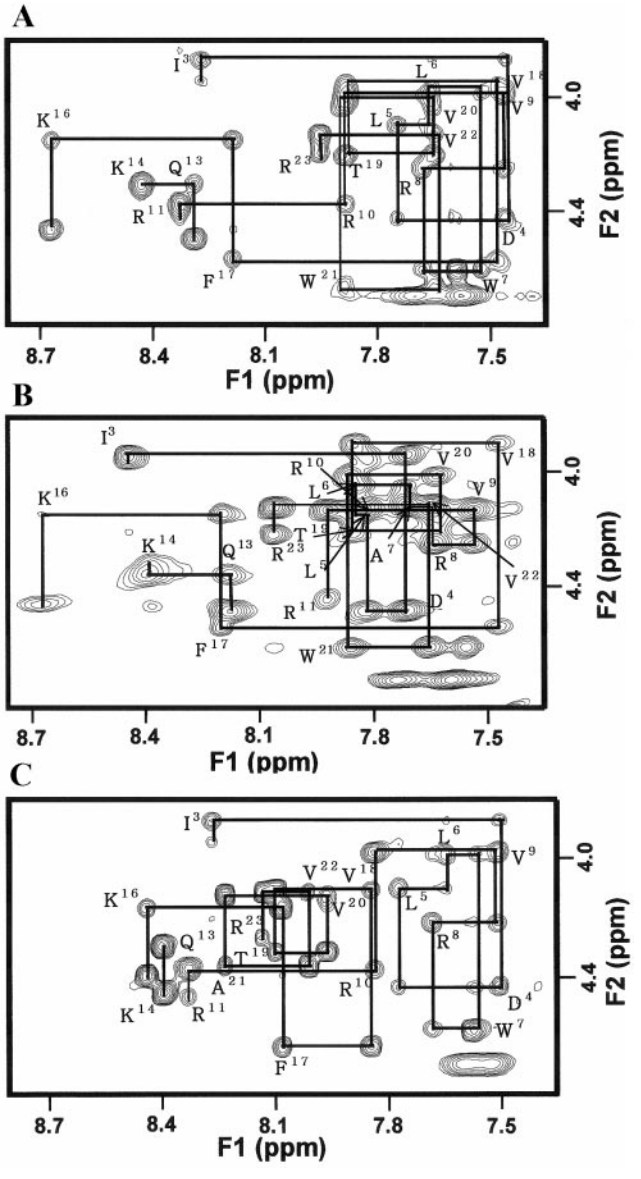

FIG. 2. NH-CαH region of a 250-ms mixing time NOESY spectrum of (A) PMAP-23, (B) PMAP-1, and (C) PMAP-2. For the sake of clarity, only the intraresidual NH-CαH cross peaks are labeled.

RESULTS AND DISCUSSION

Circular Dichroism Study

To investigate the secondary structures of PMAP-23 and its analogues in membrane mimetic environments, CD spectra were measured in aqueous buffer, TFE/water solution, SDS micelles, and DPC micelles. As shown in Fig. 1, in aqueous buffer, PMAP-23 does not have any specific secondary structures. Also, in SDS micelles, PMAP-23 and its analogues do not have any specific secondary structures. Addition of TFE increases the content of α-helical structure in PMAP-23. In DPC micelles, PMAP-23 and its analogues have partial α-helical structures. However, the content of α-helix in PMAP-2 is much lower than those of PMAP-23 and PMAP-1 in TFE/water solution and DPC micelle.

Resonance Assignment and Secondary Structure

Sequence specific resonance assignment was determined using mainly DQF-COSY, TOCSY, and NOESY data (35). Figure 2 shows the NOESY spectra with the sequential assignments of PMAP-23, PMAP-1 and PMAP-2 in the NH-C_αH region. NOESY and TOCSY experiments at 293, 303, 313, and 323K allowed the complete assignment of the overlapping peaks. Chem-

TABLE 2

^{1}H Chemical Shifts (ppm)[a] in DPC Micelles

Residue	NH	αH	βH	Others
		(a) PMAP-23 (303K, pH 3.58)		
Arg[1]				
Ile[2]	9.58	3.94	2.00	γ_2:1.78, 1.64 γ^*_1:1.31 δ^*:0.94
Ile[3]	8.23	3.85	1.75	γ^*_2:1.43 γ^*_1:1.29 δ:0.92
Asp[4]	7.46	4.42	*2.80	
Leu[5]	7.75	4.07	1.90, 1.82	γ:1.57 δ^*_2:0.95 δ^*_1:0.88
Leu[6]	7.65	4.00	1.68, 1.60	γ:1.39 δ^*_2:0.86 δ^*_1:0.76
Trp[7]	7.52	4.59	3.49, 3.31	HE_3:7.58, HD_1:7.30
Arg[8]	7.88	4.24	2.00, 1.87	γ^*:1.61 δ^*:3.17 ϵ:7.42
Val[9]	7.46	3.99	2.21	γ^*_2:1.02 γ^*_1:0.96
Arg[10]	7.88	4.37	1.85, 1.74	γ:1.61 δ:3.17 ϵ:7.41
Arg[11]	8.32	4.42	*1.79	γ^*:1.65 ϵ:7.48
Pro[12]		4.49	2.22, 2.01	δ_2:3.83 δ_1:3.53
Gln[13]	8.29	4.30	*1.94	γ^*:2.36
Lys[14]	8.43	4.34	*1.75	γ^*:1.39 δ^*:1.67 ϵ^*:2.96 ζ^*:7.57
Pro[15]		4.47	2.23, 1.94	δ_2:3.90 δ_1:3.42
Lys[16]	8.66	4.15	*1.78	γ^*:1.41 δ^*:1.61 ϵ^*:2.96 ζ^*:7.57
Phe[17]	8.18	4.56	*3.13	
Val[18]	7.48	3.95	2.03	γ^*_2:0.84 γ^*_1:0.79
Thr[19]	7.89	4.20	3.94	γ^*:1.13
Val[20]	7.65	4.03	2.05	γ^*_2:0.88 γ^*_1:0.77
Trp[21]	7.89	4.65	3.31, 3.18	HE_3:7.57,HD_1:7.24
Val[22]	7.64	4.13	2.10	γ^*:0.88
Arg[23]	7.95	4.18	1.86, 1.75	γ^*:1.60 δ^*:3.16 ϵ:7.36
		(b) PMAP-1 (303K, pH 3.29)		
Arg[1]				
Ile[2]	9.50	3.96	2.00	γ_2*:1.62 γ_1*:1.30 δ*:0.95
Ile[3]	8.45	3.93	1.91	γ_2*:1.51 γ_1*:1.32 δ*:0.90
Asp[4]	7.71	4.82	*2.87	
Leu[5]	7.81	4.12	1.87, 1.78	γ:1.60 δ^*_2:0.91 δ^*_1:0.84
Leu[6]	7.84	4.05	*1.81	γ:1.57 δ^*_2:0.84 δ^*_1:0.78
Ala[7]	7.78	4.10	*1.49	
Arg[8]	7.64	4.25	2.02, 1.94	γ^*:1.79 δ^*:3.16 ϵ:7.40
Val[9]	7.53	4.13	2.25	γ^*:1.00
Arg[10]	7.85	4.21	1.87, 1.76	γ^*:1.59 δ^*:3.25 ϵ:7.52
Arg[11]	7.92	4.44	1.86, 1.79	γ^*:1.59 δ^*:3.21 ϵ:7.43
Pro[12]		4.48	2.21, 2.00	δ_2:3.77 δ_1:3.55
Gln[13]	8.18	4.36	*1.93	γ^*:2.33
Lys[14]	8.38	4.32	2.09, 1.92	γ^*:1.40 δ^*:1.73 ϵ^*:2.92 ζ^*:7.8111
Pro[15]		4.46	2.23, 1.94	δ_2:3.84 δ_1:3.50
Lys[16]	8.67	4.14	*1.78	γ^*:1.44 ϵ^*:2.95 ζ^*:7.71
Phe[17]	8.20	4.54	*3.13	
Val[18]	7.47	3.89	2.02	γ_2*:0.84 γ_1*:0.80
Thr[19]	7.85	4.17	3.88	γ^*:1.16
Val[20]	7.63	4.01	2.04	γ_2*:087 γ_1*:0.77
Trp[21]	7.86	4.61	3.30, 3.16	HE_3:7.43 HD_1:7.55
Val[22]	7.65	4.12	2.11	γ^*:0.89
Arg[23]	8.06	4.21	1.87, 1.78	γ^*:1.61 δ^*:3.16 ϵ:7.49
		(c) PMAP-2 (303K, pH 3.00)		
Arg[1]				
Ile[2]	9.56	3.94	2.00	γ_2:1.77, 1.64 γ^*_1:1.30 δ^*:0.94
Ile[3]	8.27	3.87	1.87	γ_2*:1.47 γ_1*:1.27 δ:0.90
Asp[4]	7.51	4.43	*2.81	
Leu[5]	7.77	4.07	1.88, 1.80	γ:1.57 δ^*_2:0.94 δ^*_1:0.88
Leu[6]	7.64	3.98	1.65, 1.59	γ:1.39 δ^*_2:0.83 δ^*_1:0.73
Trp[7]	7.58	4.58	3.42, 3.29	HE_3:7.59 HD_1:7.31
Arg[8]	7.68	4.21	1.96, 1.85	δ^*:3.16 ϵ:7.42
Val[9]	7.51	3.98	2.19	γ^*:1.00
Arg[10]	7.83	4.37	1.84, 1.71	γ^*:1.61 δ^*:3.12 ϵ:7.42
Arg[11]	8.33	4.46	1.82, 1.74	γ^*:1.64 δ^*:3.14 ϵ:7.48
Pro[12]		4.45	*2.25	δ_2:3.78 δ_1:3.56
Gln[13]	8.39	4.29	2.04, 1.91	γ^*:2.35
Lys[14]	8.33	4.45	*1.77	γ^*:1.43 δ^*:1.68 ϵ^*:2.90
Pro[15]		4.39	2.21, 1.93	δ_2:3.840 δ_1:3.53
Lys[16]	8.44	4.16	*1.69	γ^*:1.30 δ^*:1.39 ϵ^*:2.90
Phe[17]	8.08	4.63	*3.08	
Val[18]	7.84	4.10	2.02	γ^*:0.84
Thr[19]	8.10	4.31	2.01	γ^*:1.17
Val[20]	7.96	4.12	2.06	γ^*:0.90
Ala[21]	8.23	4.36	*1.34	
Val[22]	8.00	4.11	2.08	γ:0.92
Arg[23]	8.13	4.26	1.87, 1.75	γ^*:1.60 δ^*:3.18 ϵ:7.28

[a] Chemical shifts are relative to DSS (0 ppm).

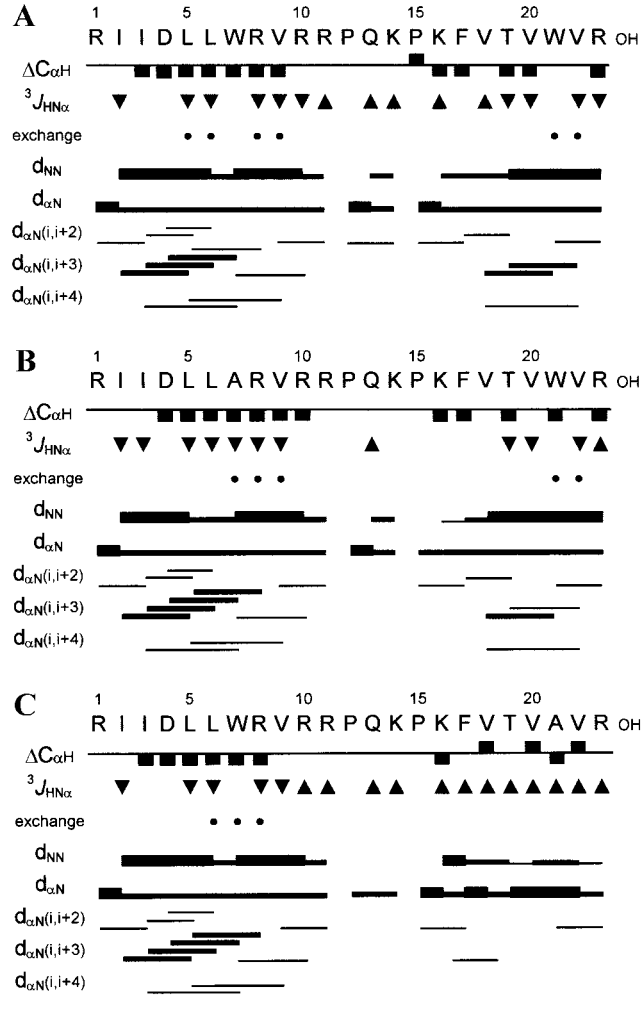

FIG. 3. Summary of the NOE connectivities, the $J_{HN\alpha}$ coupling constants (▼, $J_{HN\alpha} < 6$ Hz), amide exchange and the CαH chemical shift index for (A) PMAP-23, (B) PMAP-1, and (C) PMAP-2 in DPC micelles. Circles in the exchange row denote slowly exchanged amide protons, which are still visible after 2 h in D_2O. Line thinkness for the NOEs reflects the intensity of the NOE connectivities.

ical shifts of PMAP-23 and its analogues in DPC micelle at 303K, at pH 4.0, referenced to DSS, are listed in Table 2. The overall chemical shift of PMAP-23 is similar to those of its analogues, except in the region with a substitution.

The sequential NOE connectivities and the other NMR data are illustrated in Fig. 3. As shown in Figs. 2 and 3, a number of nonsequential NOE connectivities which are the characteristics of α-helix, i.e., $d_{\alpha N}(i, i+3)$, and $d_{\alpha Ni}(i, i+4)$ correlations from Ile2 to Arg10, have been observed for the N-terminus of PMAP-23 and its analogues. For the PMAP-23 and PMAP-1, there are $d_{\alpha N}(i, i+3)$, and $d_{\alpha N}(i, i+4)$ correlations in the C-terminal region, while PMAP-2 does not have these correlations in the C-terminal regions, which are characteristics of the α-helix.

TABLE 3

Structural Statistics and Mean Pairwise rmsds for the 20 Lowest Structures of PMAP-23 and Its Analogues in DPC Micelles[a]

	PMAP-23	PMAP-1	PMAP-2
Experimental distance restraints			
Total	173	155	150
Sequential	84	80	75
Medium range	32	25	24
Intraresidue	57	50	51
Dihedral angle restraints	15	12	17
rmsd from experimental restraints			
NOE (Å)	0.044 ± 0.002	0.040 ± 0.003	0.043 ± 0.002
ϕ (deg)	0.249 ± 0.090	0.304 ± 0.069	0.119 ± 0.093
rmsd from convalent geometry			
Bonds (Å)	0.003 ± 0.0001	0.002 ± 0.0002	0.003 ± 0.0001
Angles (deg)	0.528 ± 0.008	0.519 ± 0.011	0.523 ± 0.009
Impropers (deg)	0.346 ± 0.007	0.362 ± 0.007	0.362 ± 0.009
Average energies (kcal mol^{-1})			
E_{tot}	63.8 ± 2.2	55.7 ± 3.4	59.2 ± 2.1
E_{NOE}	19.5 ± 1.7	14.5 ± 2.3	16.5 ± 1.7
E_{tor}	0.07 ± 0.05	0.08 ± 0.04	0.02 ± 0.02
E_{repel}	1.48 ± 0.45	1.49 ± 1.07	2.23 ± 0.81
rmsd from the mean structure			
Backbone atoms of all residues	3.07 ± 0.69	3.02 ± 0.54	3.13 ± 0.77
All heavy atoms of all residues	4.57 ± 0.72	4.52 ± 0.49	4.59 ± 0.82
Backbone atoms of N-terminal residues (1–10)	0.38 ± 0.12	0.41 ± 0.12	0.38 ± 0.11
All heavy atoms of N-terminal residues (1–10)	1.38 ± 0.30	1.62 ± 0.45	1.37 ± 0.27

[a] E_{NOE}, E_{tor}, and E_{repel} are the energies related to the NOE violations, the torsion angle violations, and the van der Waals repulsion term, respectively. Values of the square-well NOE (E_{NOE}) and torsion angle (E_{tor}) potentials are calculated with force constants of 50 kcal mol^{-1} Å^{-2} and 200 kcal mol^{-1} rad^{-2}, respectively. Values of the quartic van der Waals repulsion term (E_{repel}) are calculated with a force constant of 4 kcal mol^{-1} Å^{-4}. The rmsd values were obtained by best fitting the backbone atom (N, Cα, C′, O) coordinates for all residues of the 20 converged structures. Numbers given for the backbone and all heavy atoms represent mean values ± standard deviations.

The observed values of the $^3J_{HN\alpha}$ coupling constant for the helical region in the N-terminus of all of the peptides are generally less then 6 Hz, as shown in Fig. 3. The values of the amide proton temperature coefficient have been used to predict hydrogen bond donors, and values more positive than −4.5 ppb/K can be taken as an indicator that the amide proton is involved in intramolecular hydrogen bonding (36). Temperature coefficients of the amide protons in the N-terminal regions of PMAP-23 and its analogues are generally more positive than −4.5 ppb/K and this result indicates that the N-terminal regions of these peptides form α-helices. Also, a dense grouping of four or more −1 chemical shift index values that is not interrupted by a +1 indicates the presence of an α-helix in this region (37). The presence of small $^3J_{HN\alpha}$ coupling constants, the sequence of residues with chemical shift indices of −1, the temperature coefficients, and the NOE patterns present strong evidences that PMAP-23 and its analogues have a stable helical structure in the N-terminus. However, only PMAP-23 and PMAP-1 have short α-helices in the C-terminal region.

Tertiary Structures

To determine the tertiary structures of PMAP-23 and its analogues, we used experimental restraints such as sequential ($|i - j| = 1$), medium-range ($1 < |i - j| \leq 5$), long-range ($|i - j| > 5$), intraresidual distance, and torsion angle restraints, as listed in Table 3. From the structures, which were accepted with a small deviations from idealized covalent geometry and experimental restraints (≤0.05 Å for bonds, ≤5° for angles, ≤5° for chirality, ≤0.3 Å for NOE restraints, and ≤3° for torsion angle restraints), and 20 output structures with the lowest energy for each peptides were analyzed.

The statistics of the 20 final simulated annealing (SA) structures of PMAP-23 and its analogues are given in Table 3. All 20 SA structures displayed good covalent geometries and small NMR constraint violations. When we superimpose the 20 structures of each peptide on the backbone atoms of residues from Arg1 to Arg10, their rms deviations from the mean structure are 0.38–0.41 Å for the backbone atoms (N, Cα, C′, O) and 1.37–1.62 Å for all heavy atoms. However, the rms deviations for all residues from the mean structures are much bigger for all peptides because of the flexible region in the middle.

Figure 4 shows the ribbon diagram of the lowest energy structures of PMAP-23 and its analogues. In Fig. 5, all heavy atoms from Arg1 to Arg10 of 20 structures were superimposed with respect to the

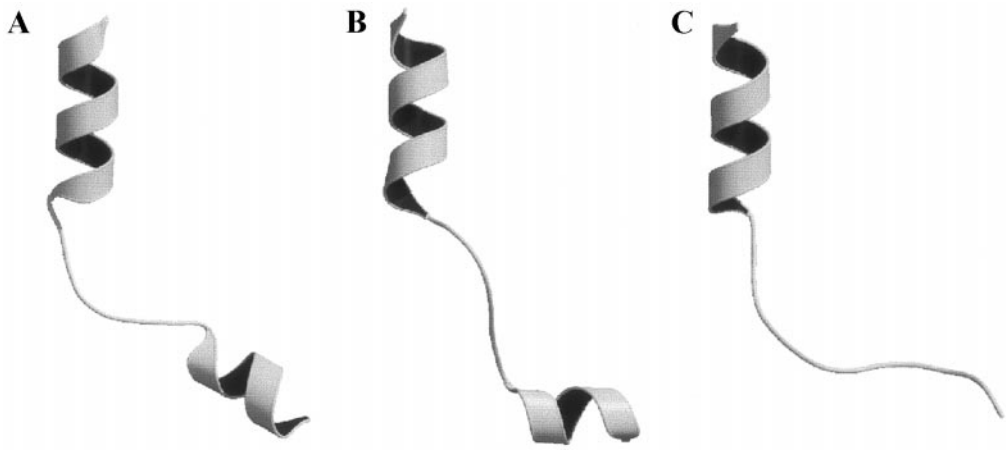

FIG. 4. Ribbon diagrams of the restrained minimized mean structure of (A) PMAP-23, (B) PMAP-1, and (C) PMAP-2.

restrained-minimized average structure for all peptides. According to the PROCHECK analysis, in PMAP-23 and PMAP-1, there is an α-helix from Arg1 to Arg10 in the N-terminal region and the short α-helix from Phe17 to Arg23 in the C-terminal region, which is connected with a flexible region containing two proline residues.

Structure–Activity Relationships

The Trp residues in melittin, mastoparan B, and cecropin A–magainin 2 hybrid peptide have been reported to be critical for their antibacterial or hemolytic activities (38–42). In mellitin and mastoparan, the Trp residues are located in the hydrophobic core of the peptides, restricted motionally in the membrane, and involved in the hydrophobic interactions with the acyl chains of the phospholipid (38–40). In case of cecropin A–magainin 2 hybrid peptide, Trp residue is located at a rather flexible region in the N-terminus and Trp in the short α-helix at the N-terminus of hybrid peptide is essential for its antibiotic activity and primary interaction with the cell membrane (41, 42). In PMAP-23 peptide, there are two Trp residues located at position 7 in the N-terminus and located at position 21 in the C-terminus.

Our previous studies showed that PMAP-1 ($Trp^{7}\rightarrow Ala$) has a similar antibiotic activity to PMAP-23, while PMAP-2 ($Trp^{21}\rightarrow Ala$) had lower activity than PMAP-23 (19). By substitution of Ala for Trp^{7}, overall structural features of PMAP-23 are retained in PMAP-1, having an amphipathic α-helix from Arg1 to Arg10 in the N-terminal region and a short α-helix from Phe^{17} to Arg^{23} in the C-terminal region. However, by substitution of Ala for Trp^{21}, the α-helix in the C-terminal region is disappeared in PMAP-2, while an α-helix with about three turns in the N-terminal region

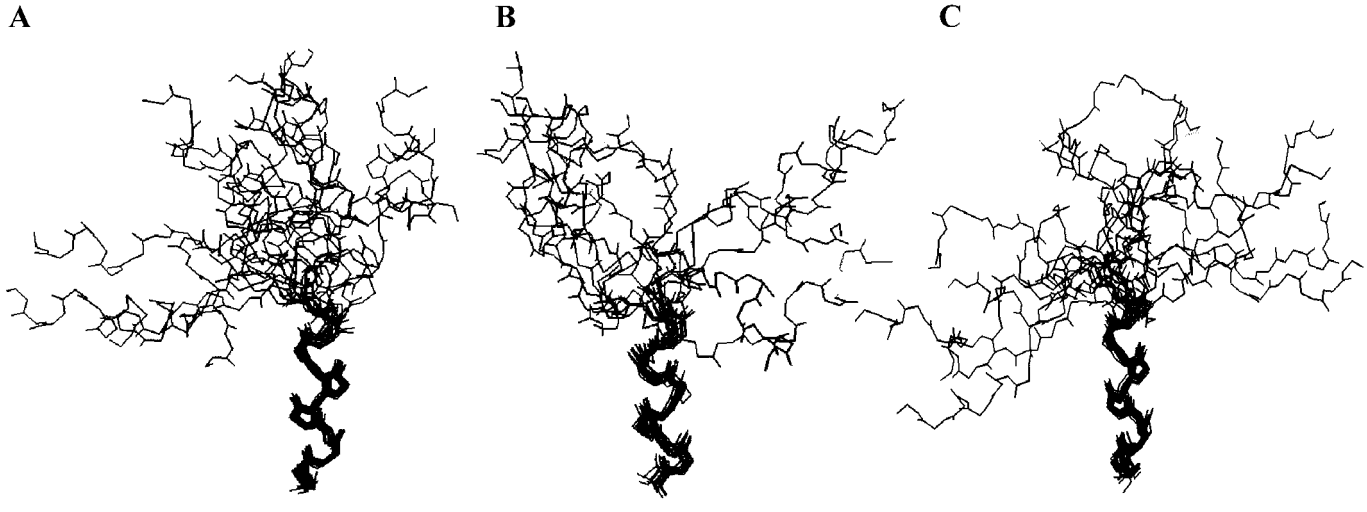

FIG. 5. The superpositions of the 20 lowest energy structures calculated from the NMR data, using backbone atoms of residues 1–10. (A) PMAP-23, (B) PMAP-1, and (C) PMAP-2.

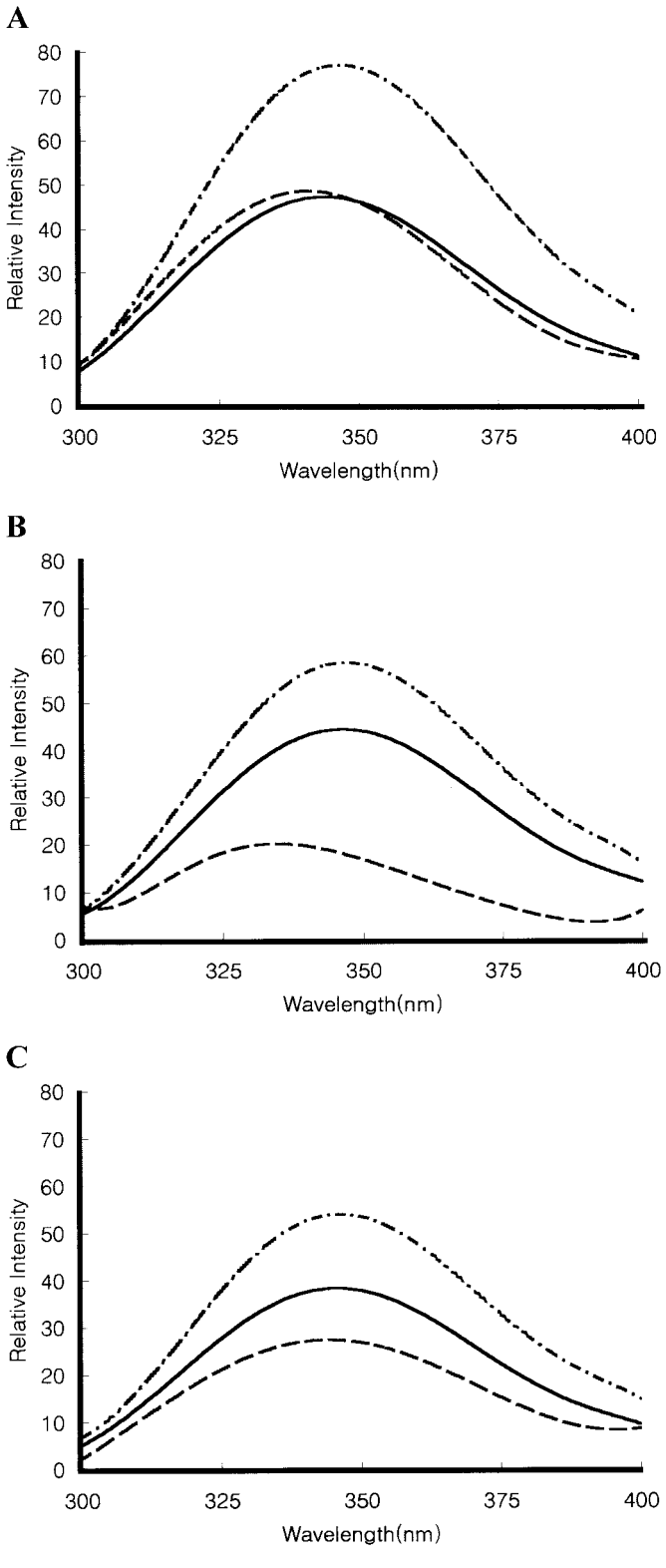

FIG. 6. Fluorescence spectra of (A) PMAP-23, (B) PMAP-1, and (C) PMAP-2 in PC vesicle (—), PC/PS (4:1, w/w) vesicle (···), and phosphate buffer (– · –).

is retained. Figure 6 shows the fluorescence spectra of PMAP-23, PMAP-1, and PMAP-2. Tryptophan fluorescence shows high sensitivity to the polarity of the membrane environment. Fluorescence spectra of peptide in phosphate buffer has emission maximum at 346 nm. When we added the neutral vesicle such as PC to the peptide solution, it did not show any blue shift. When the peptides are bound to PC/PS anionic vesicle, a membrane-mimicking environment, there were more remarkable blue shifts in PMAP-23 and PMAP-1 compared to PMAP-2. Therefore, this result suggested that Trp^{21} in PMAP-23 has stronger interaction with phospholipids than Trp^{7} because insertions of Trp21 indole ring deep into the acyl chains of the phospholipid results in a blue shift of Trp fluorescence emission.

We have reported that Pro^{15}→Ala substitution and Pro^{12}→Ala substitution in PMAP-23 caused a decrease in liposome-disrupting and antitumor activities compared PMAP-23 (43). In the case of the cecropin A–magainin 2 hybrid peptide, the flexibility or bending potential induced by the hinge region in the central part of the peptides plays important role in their antibiotic activities and may allow the α-helix in the C-terminus to span the lipid bilayer (41, 42). Therefore, the flexible region including two proline residues in the middle of PMAP-23 may be important for the antibiotic activities in PMAP-23, too.

CONCLUSION

According to the three-dimensional structure, PMAP-23 and PMAP-1 have similar structures and both have an α-helix with about three turns in the N-terminal region, a short α-helix in the C-terminal region, and a flexible region in between the two helices. However, PMAP-2 has an α-helical structure only in the N-terminal region and has a flexible structure in the C-terminal region. A Trp^{21}→Ala substitution (PMAP-2) in PMAP-23 resulted in more significant reduction on antibacterial activity and liposome-disrupting activity compared to Trp^{7}→Ala substitution (PMAP-1) (19). Because Ala^{21} residue in PMAP-2 couldn't make effective interaction with membrane surface, PMAP-2 doesn't have effective antibacterial activities. All the results imply that Trp^{21} is important for inducing an α-helix in the C-terminal region and Trp^{21} may plays important role on antibiotic activity of PMAP-23. Also, the blue shift experiment showed that Trp^{21}-residue in PMAP-23 is more accessible to hydrophobic tail of phospholipid vesicles than Trp^{7}.

Therefore, Trp^{21} residue at the C-terminus of PMAP-23 are important for the primary binding to the membrane, and then the amphipathic short helix at the C-terminus of PMAP-23 is induced. Also, the C-terminal end of PMAP-23 penetrates into the lipid bilayers.

The flexible region including two proline residues may allow the α-helix in the C-terminus to span the lipid bilayer.

ACKNOWLEDGMENTS

This work was financially supported by a grant from the Korean Research Foundation (KRF-1999-015-DI0070) and a grant from the Ministry of Science and Technology, Korea, and the Korea Science and Engineering Foundation through the Research Center for Proteineous Materials.

REFERENCES

1. Zasloff, M. (1992) Antibiotic peptides as mediators of innate immunity. *Curr. Opin. Immunol.* **4,** 3–7.
2. Boman, H. G. (1995) Peptide antibiotics and their role in innate immunity. *Annu. Rev. Immunol.* **13,** 61–92.
3. Hancock, R. E., and Lehrer, R. I. (1998) Cationic peptides: A new source of antibiotics. *Trends Biotechnol.* **16,** 82–88.
4. Gallo, R. L., Kim, K, J., Bernfield, M., Kozak, C. A., Zanetti, M., Merluzzi, L., and Ganz, T., and Lehrer, R. I. (1997) Antimicrobial peptides of leukocytes. *Curr. Opin. Hematol.* **4,** 53–58.
5. Gudmundsson, G. H., Agerberth, H. B., Odeberg, J., Bergman, T., Olsson, B., and Salcedo, R. (1996) The human gene FALL-39 and processing of the cathelin precursor to the antibacterial peptide LL-39 in granulocytes. *Eur. J. Biochem.* **238,** 325–332.
6. Gennaro, R. (1997) Identification of CRAMP, a cathelin-related antimicrobial peptide expressed in the embryonic and adult mouse. *J. Biol. Chem.* **272,** 13088–13093.
7. Baegella, L., Scocchi, M., and Zanetti, M (1995)) cDNA sequences of three sheep myeloid cathelicidins. *FEBS Lett.* **376,** 225–228.
8. Mahoney, M. M., Lee, A. Y., Brezinski-Caliguri, D. J., and Huttner, K. M. (1995) Molecular analysis of the sheep cathelin family reveals a novel antimicrobial peptide. *FEBS Lett.* **377,** 519–522.
9. Tossi, A., Scocchi, M., Zanetti, M., Storici, P., and Gennaro, R. (1995) Porcine myeloid antimicrobial peptide, PMAP-37, a novel antimicrobial peptide from pig myeloid cell: cDNA cloning, chemical synthesis and activity. *Eur. J. Biochem.* **228,** 941–946.
10. Skerlavaj, B., Gennaro, R., Bagella, L., Merluzzi, L., Risso, A., and Zanetti, M. (1996) Biological characterization of two novel cathelicidin-derived peptides and identification of structural requirements for their antimicrobial and cell lytic activities. *J. Biol. Chem.* **271,** 375–381.
11. Storici, P., and Zanetti, M. (1993) A cDNA derived from pig bone marrow cells contains a sequence identical to the intestinal antimicrobial peptide PR-39. *Biochem. Biophys. Res. Commun.* **196,** 1058–1065.
12. Zanetti, M., Del Sal, G., Storici, P., Schneider, C., and Romeo, D. (1993) The cDNA of the neutrophil antibiotic Bac5 predicts a pro-sequence homologous to a cysteine proteinase inhibitor, that is common to other neutrophil antibiotics. *J. Biol. Chem.* **268,** 522–526.
13. Del Sal, G., Storici, P., Schneider, C., and Romeo, D., and Zanetti, M. (1992) cDNA cloning of the neutrophil bactericidal peptide indolicidin. *Biochem. Biophys. Res. Commun.* **187,** 467–472.
14. Zhao, C., Liu, L., and Lehrer, R. I. (1994) Identification of a new member of the protegrin family by cDNA cloning. *FEBS Lett.* **346,** 285–288.
15. Zanetti, M., Gennaro, R., and Romeo, D. (1995) Cathelicidins: A novel protein family with a common proregion and a variable C-terminal antimicrobial domain. *FEBS Lett.* **374,** 1–5.
16. Panyutich, A., Shi, J., Boutz, P. L., Zhao, C., and Ganz, T. (1997) Porcine polymorphonuclear leukocytes generate extracellular microbial activity by elastase-mediated activation of secreted proprotegrins. *Infect. Immun.* **65,** 978–985.
17. Zanetti, M., Litteri, L., Griffiths, G., Gennaro, R., and Romeo, D. (1991) Stimulus-induced maturation of probactenecins, precursors of neutrophil antimicrobial polypeptides. *J. Immunol.* **146,** 4295–4300.
18. Zanetti, M., Storici, P., Tossi. A., Scocchi, M., and Gennaro, R. (1994) Molecular cloning and chemical synthesis of a novel antimicrobial peptide derived from pig myeloid cells. *J. Biol. Chem.* **269,** 7855–7858.
19. Kang, J. H., Shin, S. Y., Jang, S. Y., Kim, K. L., and Hahm, K.-S. (1999) Effects of tryptophan residues of porcine myeloid antibacterial peptide PMAP-23 on antibiotic activity. *Biochem. Biophys. Res. Commun.* **264,** 281–286
20. Merrifield, R. B. (1986) Solid phase synthesis. *Science* **232,** 341–347.
21. Derome, A., and Williamson, M., Derome, A., and Williamson, M. (1990) Rapid-pulsing artifacts in double-quantum-filtered COSY. *J. Magn. Reson.* **88,** 177–185.
22. Bax, A., and Davis, D. G. (1985) MLEV-17-based two-dimensional homonuclear magnetization transfer spectroscopy. *J. Magn. Reson.* **65,** 355–360.
23. Macura, S., and Ernst, R. R. (1980) Elucidation of cross-relaxation in liquids by two-dimensional NMR spectroscopy. *Mol. Phys.* **41,** 95–117.
24. Bax, A., and Davis, D. G. (1985) Practical aspects of two-dimensional transverse NOE spectroscopy. *J. Magn. Reson.* **63,** 207–213.
25. Marion, D., and Wüthrich, K. (1983) Application of phase sensitive two-dimensional correlated spectroscopy (COSY) for measurements of ^{1}H–^{1}H spin–spin coupling constants in proteins. *Biochem. Biophys. Res. Commun.* **113,** 967–974.
26. Muller, L. (1987) P.E.COSY, a simple alternative to E.COSY. *J. Magn. Reson.* **72,** 191–197.
27. Kim, Y., and Prestegard, J. P. (1989) Measurement of vicinal coupling from cross peaks in COSY spectra. *J. Magn. Reson.* **84,** 9–13.
28. Clore, G. M., and Gronenborn, A. M. (1989) Determination of three-dimensional structures of proteins and nucleic acids in solution by nuclear magnetic resonance spectroscopy. *CRC Crit. Rev. Biochem. Mol. Biol.* **24,** 479–564.
29. Clore, G. M., and Gronenborn, A. M. (1994) Structures of larger proteins, protein–ligand and protein–DNA complexes by multidimensional heteronuclear NMR. *Protein Sci.* **3,** 372–390.
30. Brünger, A. T. (1993) X-PLOR Manual, version 3.1, Yale Univ., New Haven, CT.
31. Wüthrich, K., Billeter, M., and Braun, W. (1983) Pseudo-structures for the 20 common amino acids for use in studies of protein conformations by measurements of intramolecular proton–proton distance constraints with nuclear magnetic resonance. *J. Mol. Biol.* **169,** 949–961.
32. Clore, G. M., Gronenborn, A. M., Nilges, M., and Ryan, C. A. (1987) Three-dimensional structure of potato carboxypeptidase inhibitor in solution. A study using nuclear magnetic resonance, distance geometry, and restrained molecular dynamics. *Biochemistry* **26,** 8012–8023.
33. Nilges, M., Clore, G. M., and Gronenborn, A. M. (1988) Determination of three-dimensional structures of proteins from interproton distance data by hybrid distance geometry–dynamical simulated annealing calculations. *FEBS Lett.* **229,** 317–324.
34. Kuszewski, J., Nilges, M., and Brünger, A. T. (1992) Sampling and efficiency of metric matrix distance geometry: A novel partial metrization algorithm. *J. Biomol. NMR* **2,** 33–56.
35. Wüthrich, K. (1986) NMR of Protein and Nucleic Acid, Wiley-Interscience, New York.
36. Baxter, N. J., and Williamson, M. P. (1997) Temperature depen-

dence of ^{1}H chemical shifts in proteins. *J. Biomol. NMR* **9,** 359–369.

37. Wishart, D. S., Sykes, B. D., and Richards, F. M. (1992) The chemical shift index: A fast and simple method for the assignment of protein secondary structure through NMR spectroscopy. *Biochemistry* **31,** 1647–1651.
38. Ghosh, A. K., Rukmini, R., and Chattopadhyay, A. (1997) Modulation of tryptophan environment in membrane-bound melittin by negatively charged phospholipids: Implications in membrane organization and function. *Biochemistry* **36,** 14291–14305.
39. Yu, K., Kang, S., Park, N., Shin, J., and Kim, Y. (1999) Relationship between the tertiary structures of mastoparan B and its analogs and their lytic activities studied by NMR spectroscopy. *J. Pept. Res.* **55,** 51–65.
40. Yu, K., Kang, S., Kim, S. D., Ryu, P. D., and Kim, Y. (2001) Interaction between mastoparan B and the membrane studied by ^{1}H NMR spectroscopy *J. Biomol. Struct. Dynam*. **4,** 595–606.
41. Oh, D., Shin, S. Y., Kang, J. H., Hahm, K.-S., Kim, K. L., and Kim, Y. (1999) NMR structural characterization of cecropin A(1–8)–magainin 2(1–12) and cecropin A(1–8)–melittin(1–12) hybrid peptides *J. Pept. Res.* **53,** 578–589.
42. Oh, D., Shin, S. Y., Lee, S., Kang, J. H., Kim, S. D., Ryu, P. D., Hahm, K.-S., and Kim, Y. (2000) Role of the hinge region and the tryptophan residue in the synthetic antimicrobial peptides, cecropin A(1–8)–magainin 2(1–12) and its analogues, on their antibiotic activities and structures. *Biochemistry* **39,** 11855–11864.
43. Shin, S. Y., Kang, J. H., Jang, S. Y., Kim, K. L., and Hahm K.-S. (2000) Structure and antibiotic activity of a porcine myeloid antimicrobial peptide, PMAP-23 and its analogues. *J. Biochem. Mol. Biol.* **33,** 49–53.